Volume 4 | Number 36 | 28 September 2016 | Pages 13663–14034

# Journal of Materials Chemistry A

Materials for energy and sustainability

www.rsc.org/MaterialsA

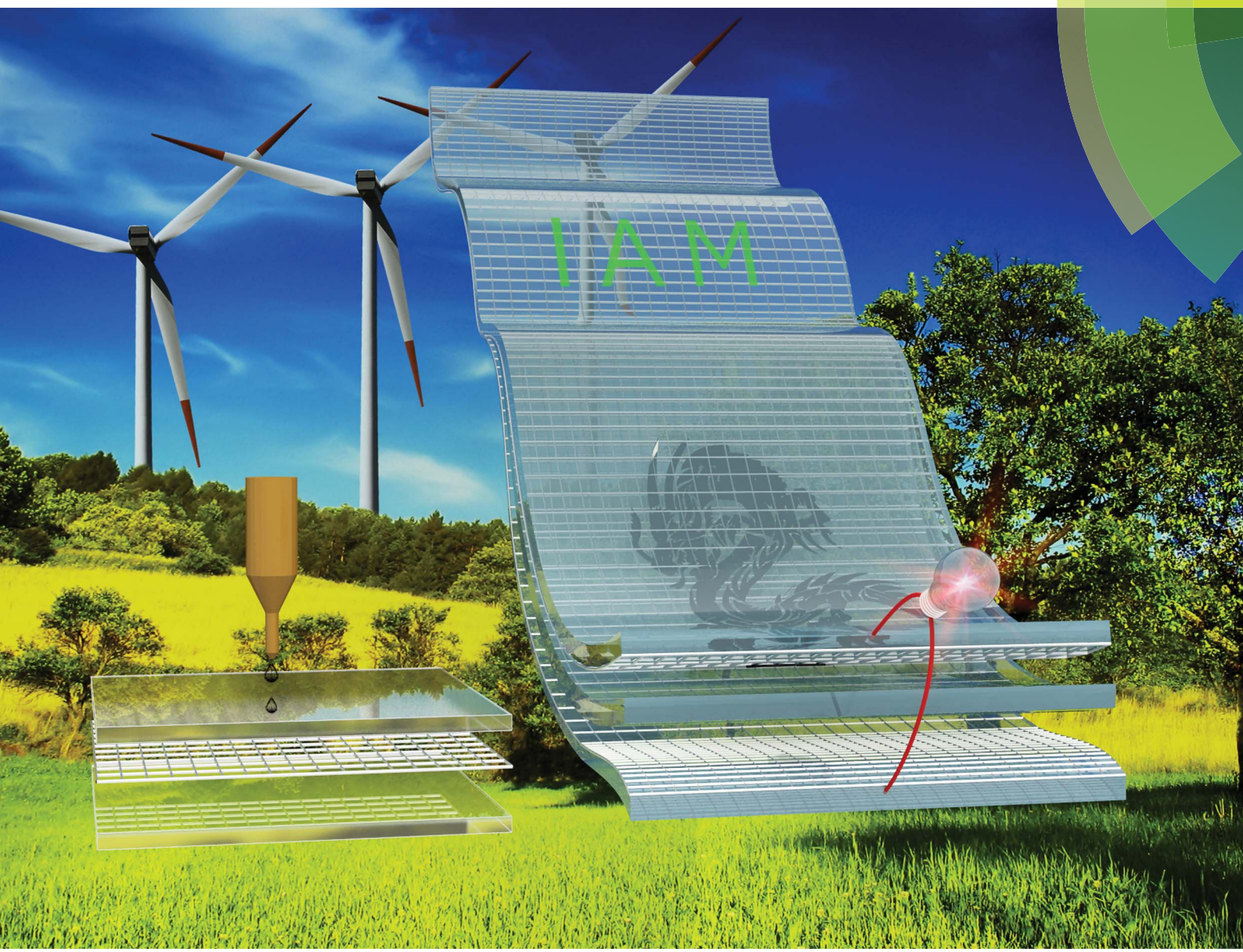


ISSN 2050-7488

ROYAL SOCIETY OF CHEMISTRY

PAPER

Wen-Yong Lai *et al.*

Inkjet-printed flexible, transparent and aesthetic energy storage devices based on PEDOT:PSS/Ag grid electrodes

175 YEARS

Journal of Materials Chemistry A

PAPER

Cite this: J. Mater. Chem. A, 2016, 4, 13754

# Inkjet-printed flexible, transparent and aesthetic energy storage devices based on PEDOT:PSS/Ag grid electrodes†

Tao Cheng,[a] Yi-Zhou Zhang,[a] Jian-Peng Yi,[a] Lei Yang,[a] Jian-Dong Zhang,[a] Wen-Yong Lai*[ab] and Wei Huang[ab]

Flexible transparent PEDOT:PSS/Ag grids were inkjet printed on polyethylene terephthalate substrates. The combination of Ag grids with PEDOT:PSS not only compensates for the demerits of the single materials but also makes full use of their advantages. The Ag grids and the PEDOT:PSS layer offered extra conductive paths for each other, yielding a much lower sheet resistance of the PEDOT:PSS/Ag grids than that of either the Ag grids or the PEDOT:PSS layer, thus improving the electrochemical performance as well. The PEDOT:PSS layer could also boost the anti-oxidation capability as well as smoothen the line of the Ag grids. Various exquisite patterns of the modified PEDOT:PSS were inkjet printed on the delicate Ag grids, forming an aesthetic appearance. As a result, the PEDOT:PSS/Ag grid hybrid electrodes exhibited superior optoelectronic performance ($T$ ~89% and $R_s$ ~12 Ω sq$^{-1}$), very good electrochemical energy storage behaviours, high flexibility and delicate patterns. Inkjet-printed flexible transparent all-solid-state supercapacitors have thus been constructed with both aesthetic appearance and superior electrochemical performance for the first time using the resultant PEDOT:PSS/Ag grids as both current collectors and active electrode materials.

Received 24th June 2016
Accepted 8th August 2016

DOI: 10.1039/c6ta05319j

www.rsc.org/MaterialsA

## Introduction

Energy conversion and storage devices play important roles in modern human society as renewable power sources.[1–4] Particularly, flexible and transparent energy conversion and storage devices that not only possess superior mechanical flexibility but also exhibit high optical transparency represent the technological frontier and have attracted extensive attention in both academia and industry.[5–15] Typical examples include flexible/wearable and transparent solar cells and supercapacitors that can intimately cling to clothes or handbags to charge mobile phones anytime and anywhere, or mounted on windows as integrated power sources for buildings, automobiles and even for spaceships. As the fundamental components of these devices, electrode materials undoubtedly have a great impact on the device performance. In this regard, the search for ideal electrode materials that simultaneously show superior optoelectronic performance and very good electrochemical energy storage behaviours is of significance and is essential for flexible and transparent energy conversion and storage devices. However, it is challenging to develop such an ideal electrode material due to the lack of effective strategies to combine all the merits of existing electrode materials.

Metal nanowires,[16–20] carbon nanotubes,[21] graphene,[22] poly(3,4-ethylenedioxythiophene):poly(styrene sulfonate) (PEDOT:PSS),[23–25] and metal grids[26] have recently offered a novel paradigm for flexible transparent electrodes. Although carbon nanomaterials show excellent flexibility and very good electric double-layer capacitor behaviours, the optoelectronic performance is usually limited by their relatively low conductivity.[27] Consequently, a thick film is required to improve the conductivity, which is detrimental to the optical transmittance. PEDOT:PSS, a typical pseudocapacitive material, possesses a variety of advantages, including high optical transparency, superior flexibility, and excellent chemical stability, but it also suffers from moderate electrical conductivity, unfavourable for achieving high optoelectronic performance.[28] Thin-film electrodes based on metal nanowire networks[17] or metal grids[26] with high flexibility and superior optoelectronic performance have been reported, but their limited electrochemical energy storage behaviours restrict their application in supercapacitors. Apparently, electrode materials with superior optoelectronic performance usually lack good electrochemical energy behaviours while electrode materials with superb capacitor behaviours commonly suffer from relatively poor optoelectronic performance, which is detrimental to transparent energy conversion and storage devices, especially transparent supercapacitors.

[a]Key Laboratory for Organic Electronics & Information Displays (KLOEID) & Institute of Advanced Materials (IAM), Jiangsu National Synergetic Innovation Center for Advanced Materials (SICAM), Nanjing University of Posts & Telecommunications, 9 Wenyuan Road, Nanjing 210023, China. E-mail: iamwylai@njupt.edu.cn

[b]Key Laboratory of Flexible Electronics (KLOFE) & Institute of Advanced Materials (IAM), Jiangsu National Synergetic Innovation Center for Advanced Materials (SICAM), Nanjing Tech University, 30 South Puzhu Road, Nanjing 211816, China

† Electronic supplementary information (ESI) available. See DOI: 10.1039/c6ta05319j

An ideal combination of electrode materials that show superior optoelectronic performance with electrode materials that have very good capacitor behaviours would be of great promise in developing a novel class of multifunctional electrode materials to combine all the merits. Such hybrid electrodes are not only suitable for optoelectronic energy conversion devices but also for transparent electrochemical energy storage devices, and desirable for improving renewable energy systems for modern human society. Recently, hybrid electrodes based on metal nanowires/graphene,[29] carbon nanotubes/metal nanowires,[30] PEDOT:PSS/metal grids,[31] PEDOT:PSS/metal nanowires,[32] and graphene/metal grids[33] with superb optoelectronic performance have been reported. However, these works only concentrated on the optimization of the optoelectronic performance and the electrochemical energy storage behaviours remain unexplored. Nevertheless, the simultaneous optimization of optoelectronic performance and electrochemical energy storage behaviours is exceedingly significant and urgent for developing flexible and transparent energy conversion and storage devices.

In this work, flexible transparent hybrid electrodes composed of PEDOT:PSS and Ag grids were prepared *via* low-cost and facile inkjet printing. Not only the optoelectronic performance but also the electrochemical energy storage behaviours, the flexibility, the morphology and the chemical stability of the hybrid electrodes were systematically studied. The combination of Ag grids with PEDOT:PSS not only compensated for the demerits of the single materials but also fully combined their advantages. The Ag grid and the PEDOT:PSS offered extra conductive paths for each other, leading to a much lower sheet resistance of the PEDOT:PSS/Ag grid than that of either the Ag grid or the PEDOT:PSS. The high optical transparency of both the single Ag grid and the single PEDOT:PSS layer led to the excellent optical transparency of the hybrid electrodes comparable to that of the single materials. Apart from superior optoelectronic performance, the hybrid electrodes also have very good electrochemical energy storage behaviours. On the one hand, as a typical pseudocapacitive material, PEDOT:PSS could remedy the limitation of Ag grids that lack electrochemical energy storage behaviours. On the other hand, the electrochemical energy storage behaviours of PEDOT:PSS could be further improved by combining with Ag grids because the Ag grids reduce the sheet resistance of PEDOT:PSS. A PEDOT:PSS layer could also smoothen the surface morphology as well as enhance the anti-oxidation capability of the Ag grid. Additionally, PEDOT:PSS could be designed into a variety of exquisite patterns using the inkjet printing methodology. The delicate lines of the Ag grid and the exquisite patterns of the PEDOT:PSS together defined the aesthetic appearance of the resultant PEDOT:PSS/Ag grids. Employing the inkjet-printed PEDOT:PSS/Ag grids, flexible transparent all-solid-state supercapacitors with aesthetic appearance, comparatively high optical transparency and superior electrochemical performance were fabricated. To the best of our knowledge, this is the first report on aesthetic supercapacitors using inkjet-printed PEDOT:PSS/Ag grids as both current collectors and electrode materials, which paves the way to fully inkjet-printed wearable and transparent energy storage devices.

# Experimental

### Fabrication of the PEDOT:PSS/Ag grids

Polydimethylsiloxane (PDMS)/polyethylene terephthalate (PET) substrates were prepared by spin coating liquid PDMS (the "base" and the "curing agent" at a mass ratio of 10 : 1) on cleaned PET substrates at 8000 rpm followed by curing on a hot plate at 120 °C for ~15 min. To enhance the wettability of PDMS/PET, it was treated with plasma for ~3 s. The substrate was then put on the platen of a printer and heated at 55 °C. The pre-set value of the line width was 10 μm, the drop spacing was 50 μm and the pitch ranged from 500 μm to 1000 μm. Ag grids were inkjet printed followed by annealing at 120 °C for 1 h. A PEDOT:PSS (pH 1000) solution was filtered through a syringe filter with a hole diameter of 220 nm followed by addition of 6 vol% ethylene glycol (EG) and 2 vol% surfactant (Triton-X 100). The 6 vol% EG and 2 vol% surfactant (Triton-X 100)-doped PEDOT:PSS (pH 1000) solution was spin-coated on the Ag grids at 500 rpm for 6 s and 1500 rpm for 50 s followed by annealing at 120 °C for 15 min. For preparation of the aesthetic PEDOT:PSS/Ag grids, the doped PEDOT:PSS was inkjet printed into various patterns at a drop spacing of 40 μm. The patterns, the drop spacing and the layers of the printed PEDOT:PSS were set before printing.

### Preparation of the all-solid-state supercapacitors

A gel electrolyte was prepared by mixing PVA powder (1.0 g), $H_3PO_4$ (1.0 g) and deionized water (10.0 mL). The mixture was then heated at 90 °C under stirring until it turned into a gel. The gel electrolyte was then coated on the PEDOT:PSS/Ag grids followed by drying in air at room temperature. Finally, two such electrolyte-coated PEDOT:PSS/Ag grid electrodes were assembled into a supercapacitor by pressing them together. Supercapacitors with delicate patterns were assembled using two inkjet-printed PEDOT:PSS/Ag grid electrodes as symmetrical electrodes.

# Results and discussion

The superior optoelectronic performance was successfully realized *via* reducing the line width, modulating the pitch of the Ag grids as well as combining with the modified PEDOT:PSS layer. The smaller the line width and the larger the pitch, the less the shadow loss and the higher the optical transmittance, as demonstrated by the numerical model:

$$t_{\text{shadow}} = \frac{w}{w+D} = \frac{1}{1+\dfrac{D}{w}} \tag{1}$$

where $t_{\text{shadow}}$ is the shadow loss, $w$ is the line width and $D$ is the pitch. The minimum line width could be obtained from eqn (2):

$$w = \sqrt{\frac{2\pi d^3}{3p\left(\dfrac{\theta}{(\sin\theta)^2} - \dfrac{\cos\theta}{\sin\theta}\right)}} \tag{2}$$

where $d$ is the droplet diameter, $p$ is the drop spacing and $\theta$ is the static advancing contact angle. Apparently, the drop spacing as well as the substrate wettability have a great impact on the line width. Besides, the substrate temperature greatly influences the solvent evaporation and the spreading of the printed Ag lines, thus affecting the line width as well. As illustrated in Fig. S1a,† the Ag lines printed on the PET substrate spread to as wide as ~150 μm despite the pre-set value of 10 μm. Intriguingly, the line width reduced significantly from ~150 μm to ~95 μm (Fig. S1i†) when fixing the drop spacing at 20 μm and increasing the temperature from 35 °C to 55 °C. This is because increasing the temperature can lead to fast solidification of the printed lines, restricting the spreading of the lines, which is desirable to achieve narrower line width. When the temperature was set at 55 °C and the drop spacing changed from 20 μm to 50 μm, the line width then decreased from ~95 μm to ~70 μm (Fig. S1l†). The line width could be further reduced to as narrow as ~48 μm, only about one third of the original line width without optimization, when an ultra-thin hydrophobic PDMS layer was spin-coated onto the PET substrate (PDMS/PET) followed by plasma treatment for 3 s, as illustrated in Fig. S2.† Fig. S3a and b† illustrate the variation of the line width with the drop spacing, the substrate temperature and the time of plasma treatment. Apart from optimizing the line width, Ag grids with various pitches ranging from 500 μm to 1000 μm were inkjet printed to further improve the optical transmittance. The optical transmittance was significantly improved *via* decreasing the line width and regulating the pitch compared with the Ag grids without optimization, as clearly shown in Fig. S4.† The optical transmittance of the Ag grids with pitch of 1000 μm and line width of ~48 μm printed on the PDMS/PET substrate was as high as ~93%.

However, it is commonly recognized that the optical transmittance and the electrical conductivity are paradoxical. Decreasing the line width and enlarging the pitch are beneficial for improving the optical transmittance but will reduce the line density, which is detrimental to electrical conductivity. The as-printed Ag grids actually exhibited very low and non-uniform conductivity because of the numerous non-conductive openings in the grids. To enhance the conductivity and its uniformity, a layer of modified PEDOT:PSS with improved conductivity was deposited on the grids *via* spin coating. PEDOT:PSS without modification could not much reduce the sheet resistance of the grids due to the low intrinsic conductivity. The sheet resistance of the pristine PEDOT:PSS layer with a thickness of around 110 nm and optical transmittance of ~94% was around 0.4 MΩ $sq^{-1}$. Nevertheless, the sheet resistance dramatically reduced to ~140 Ω $sq^{-1}$ when 6 vol% EG was added, and it further decreased to ~110 Ω $sq^{-1}$ when 2 vol% surfactant (Triton-X 100) was added, as illustrated in Fig. S5a and b.† The surfactant not only reduced the sheet resistance but also improved the wettability and reduced the surface tension of the PEDOT:PSS layer, which was beneficial for the subsequent spin-coating and especially the multilayer spin-coating of PEDOT:PSS onto the Ag grids, as shown in Fig. S6.† The pristine PEDOT:PSS was not suitable as an ink for inkjet printing. But the PEDOT:PSS solution with addition of 6 vol% EG and 2 vol% surfactant can be easily inkjet printed, which was vital to the subsequent patterning of the PEDOT:PSS layer. Fig. 1a–c show scanning electron microscopy (SEM) images of single Ag grids with line width of ~48 μm. As clearly shown in the magnified image (Fig. 1c), the lines were composed of loosely packed silver nanoparticles. Fig. 1d–f show SEM images of the Ag grids coated with PEDOT:PSS. It could be observed that smooth and closely packed Ag lines (Fig. 1f) were achieved compared with the single Ag grids. The results suggested that PEDOT:PSS filled in between the loosely packed Ag nanoparticles, which was favourable for decreasing the contact resistance.

The combination of the optimized Ag grids and the modified PEDOT:PSS simultaneously compensated for the demerits of the single materials and fully exploited their advantages, resulting in superior optoelectronic performance of the PEDOT:PSS/Ag grids over that of either the Ag grids or the PEDOT:PSS electrodes. On the one hand, the PEDOT:PSS filled in between the openings of the Ag grids and the interspace between the loosely packed Ag nanoparticles, sufficiently connecting the Ag grids and decreasing the contact resistance between the Ag nanoparticles, and therefore obviously improving the electrical conductivity of the Ag grids. On the other hand, Ag grids beneath the PEDOT:PSS also enhanced the electrical conductivity of PEDOT:PSS by providing extra conductive pathways. The high transparency of PEDOT:PSS/Ag grids mainly resulted from the high optical transmittance of both the optimized Ag grids and the PEDOT:PSS layer.

As illustrated in Fig. 2a and c, the sheet resistance of the PET-based PEDOT:PSS/Ag grids with various pitches was from ~13 Ω $sq^{-1}$ to ~25 Ω $sq^{-1}$ while the corresponding optical transmittance was from ~70% to ~87%. The sheet resistance of the PDMS/PET-based PEDOT:PSS/Ag grids varied from ~7 Ω $sq^{-1}$ to ~16 Ω $sq^{-1}$ and the optical transmittance from ~77% to ~89%, as shown in Fig. 2b and c. The optimum optoelectronic performance of the PDMS/PET-based PEDOT:PSS/Ag grids realized in this work was ~12 Ω $sq^{-1}$ (sheet resistance) and ~89% (optical transmittance). Fig. S7† shows photographs of the PDMS/PET-based PEDOT:PSS/Ag grids with an area of around 2 cm × 2 cm and various pitches. They all possessed delicate lines and high optical transmittance (the logo under them can be clearly seen). It should be noted that the optoelectronic performance of the PDMS/PET-based PEDOT:PSS/Ag grids was higher than that of the PET-based PEDOT:PSS/Ag grids because the line width of the former (~48 μm) was lower than that of the latter (~70 μm). The narrower line width implied weaker spreading and smaller coverage of the opaque Ag lines, facilitating higher optical transmittance. The weaker spreading also indicated thicker lines, resulting in lower sheet resistance. In other words, reducing the line width and modulating the pitch of the grid as well as combining with the modified PEDOT:PSS built an ideal balance between the optical transmittance and the sheet resistance, which optimized the figure of merit (FOM) defined as follows:

$$\frac{T^{10}}{R_s} \tag{3}$$

 

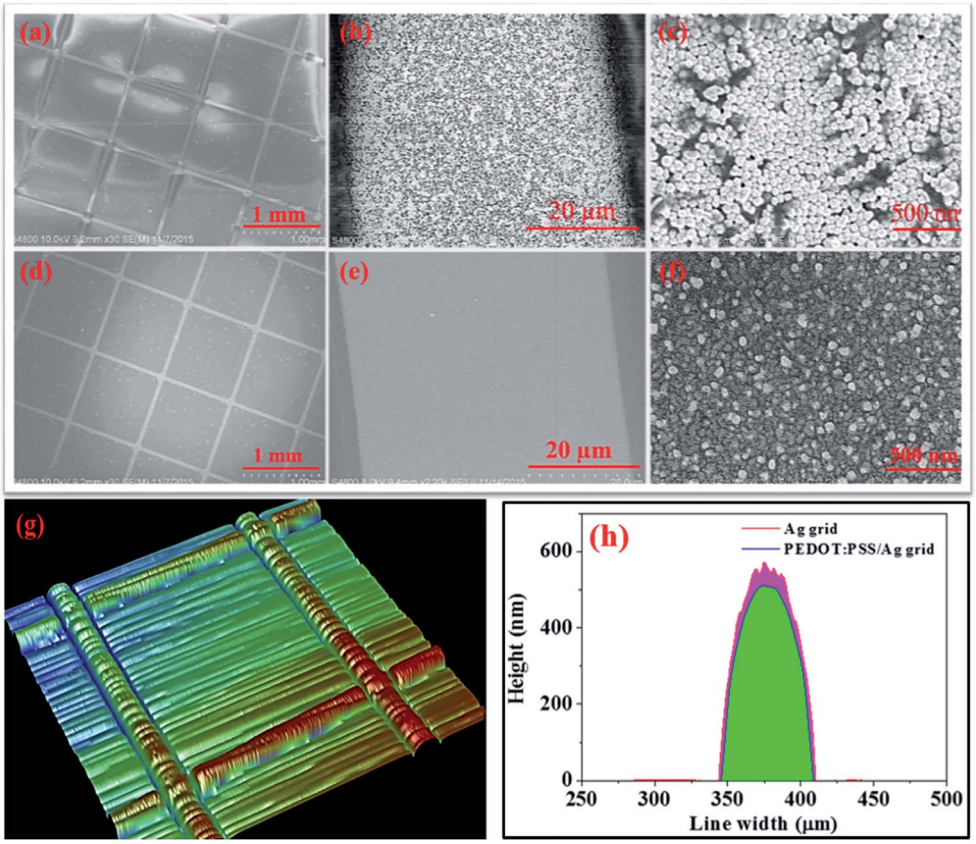


Fig. 1 Morphology of the PET/PDMS-based PEDOT:PSS/Ag grids before and after being coated with PEDOT:PSS. (a–c) SEM images of single Ag grids with different magnification. (d–f) SEM images of PEDOT:PSS/Ag grids with different magnification. (g) The 3D profile of the PET-based Ag grids. (h) The line height of the PET-based Ag grids before and after being coated with PEDOT:PSS measured with a step profiler.

As shown in Fig. 2d, the optoelectronic performance of the PDMS/PET-based PEDOT:PSS/Ag grids was comparable and even superior to that of some best-performing transparent electrodes reported in the literature,[9,16,17,19,26,29] but slightly lower than those fabricated *via* conventional methods such as nanoimprint, photolithography, wet etching and vacuum vapour deposition that are complicated, costly and energy consuming.[33–35] However, the facile solution-processed PEDOT:PSS/Ag grids in this work were cost-effective and energy-saving. Additionally, the PEDOT:PSS/Ag grids were directly annealed in air (without harsh vacuum condition) at a relatively low temperature of 120 °C to reduce the sheet resistance, leading to their compatibility with flexible PET substrates.

In most commercial inkjet-printing systems, as represented by the Dimatix 3000 system used in this work, the printing process is completed *via* the simultaneous slow transverse movement of the nozzle and the fast longitudinal movement of the platen, and thus the vertical line can be printed faster than the horizontal line. In this work, the Ag grids were inkjet printed in an ingenious way. In this process, a greatly time-saving process was devised rather than let the printer proceed following its own protocol. A series of parallel vertical lines with specific pitches were printed on the substrate followed by rotating the substrate ninety degrees and continuing to print the vertical lines, saving ~80% of the time normally needed. The Ag grids with an area of 2 cm × 2 cm and a pitch of 1000 μm could be inkjet printed within 2 min while electrohydrodynamic printed sparse grids with very small area of 100 μm × 100 μm took almost half an hour as previously reported.[36] The fast and facile inkjet printing facilitated the mass production of the Ag grids. Fig. 3a and S8† show photographs of the inkjet-printed Ag grids with a large area of about 15 cm × 13 cm.

Besides decreasing the sheet resistance of the Ag grids, the PEDOT:PSS layer also contributed to reducing the line height (the altitude of the Ag line relative to the substrate) and smoothening the surface morphology because the PEDOT:PSS filled in the openings and the interspace between the loosely packed Ag nanoparticles. For instance, the average line height of the original PET-based Ag grids was around 560 nm and the peak value was nearly 600 nm due to the protrusions on the rough surface morphology, as illustrated in Fig. 1c and h (the fluctuating red line). Fig. 1g shows the three-dimensional profile of the original Ag grids. The large line height was reduced to ~500 nm and the surface morphology became quite smooth after being coated with PEDOT:PSS, as illustrated in Fig. 1f and h (the smooth blue line).

Additionally, PEDOT:PSS usually shows superior chemical stability and it can dramatically enhance the anti-oxidation capability of the Ag grids. To demonstrate this, three samples, bare Ag film, Ag film coated with one layer of PEDOT:PSS and Ag

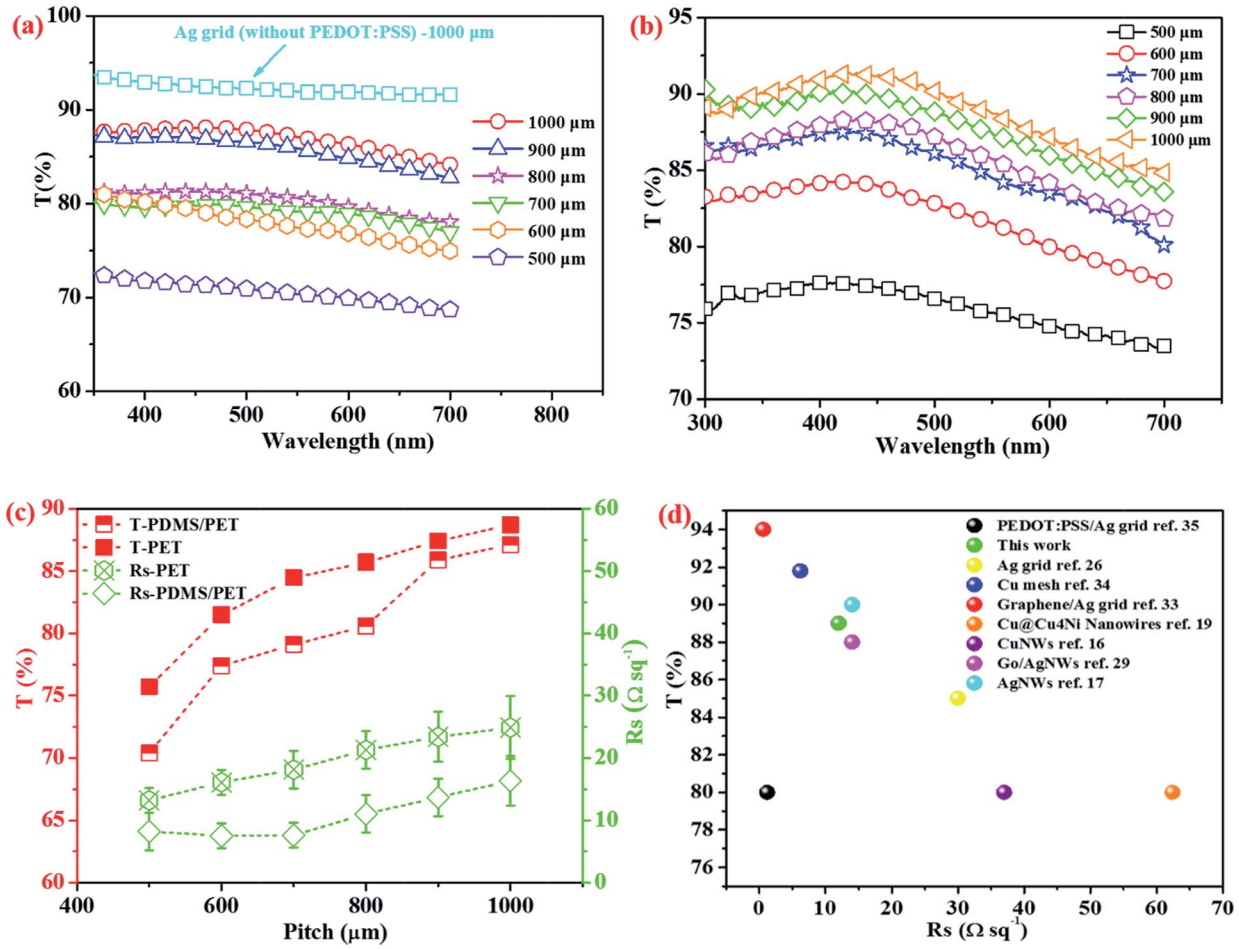


Fig. 2 Optoelectronic performance of PEDOT:PSS/Ag grids on PET and PDMS/PET substrates. (a) The optical transmittance *versus* wavelength of single Ag grids with pitch of 1000 μm and PEDOT:PSS/Ag grids with various pitches on PET substrate. (b) The optical transmittance *versus* wavelength of PEDOT:PSS/Ag grids with various pitches on PDMS/PET substrate. (c) The optical transmittance and the sheet resistance *versus* pitch of PEDOT:PSS/Ag grids on PET and PDMS/PET substrates. (d) The optoelectronic performance of the resultant PEDOT:PSS/Ag grids compared with some other best-performing transparent electrodes previously reported.

film coated with two layers of PEDOT:PSS, were left in the ultraviolet ozone (UVO) spectrometer and their sheet resistances were measured. As illustrated in Fig. 3b, the sheet resistance of the bare Ag film immediately and sharply increased in the UVO atmosphere and failed to be measurable by the four-point probe after only ~10 min. By contrast, the sheet resistance of the Ag films coated with one and two PEDOT:PSS layers only slightly increased during exposure for ~30 min. Moreover, the sheet resistance of the Ag film with two PEDOT:PSS layers increased slightly slower than that of the Ag film with one PEDOT:PSS layer. This sufficiently demonstrated that the PEDOT:PSS layer can lower the oxidation speed of the Ag grids and the thicker the PEDOT:PSS layer the more superior the anti-oxidation capability.

The sheet resistances of the PET- and PDMS/PET-based PEDOT:PSS/Ag grids were measured when they were highly bent (inset of Fig. 3d). The sheet resistance of the two hybrid electrodes slightly increased with number of times being bent, as illustrated in Fig. 3c. After being bent one hundred times, the sheet resistance only increased by 2–3 times compared with the original values, demonstrating their comparatively high flexibility, as shown in Fig. 3d. However, the flexibility was inferior to that of metal nanowire-based electrodes mainly due to the substantially longer length of metal nanowires than that of metal nanoparticles.[17]

Specific conductive area of the transparent electrode is commonly required in fabrication of optoelectronic devices. Compared with conventional materials, such as ITO, patterning is easily realized *via* inkjet printing 6 vol% EG and 2 vol% surfactant-doped PEDOT:PSS solution. Fig. S9† schematically illustrates the PEDOT:PSS/Ag grids with various patterns printed on the specific area of the substrate. To further expand the application ranges and to meet aesthetic demands, more complicated and delicate patterns, including lush bamboo, logo, and complicated circuit, were also vividly printed on the delicate Ag grids, as illustrated in Fig. 4. The superior flexibility of the electrode obviously enhanced its durability and conformability with various objects, especially with non-planar objects, as shown in Fig. 4a–c. Besides the very good flexibility, the high optical transparency and the exquisite patterns render the PEDOT:PSS/Ag grids extremely

 

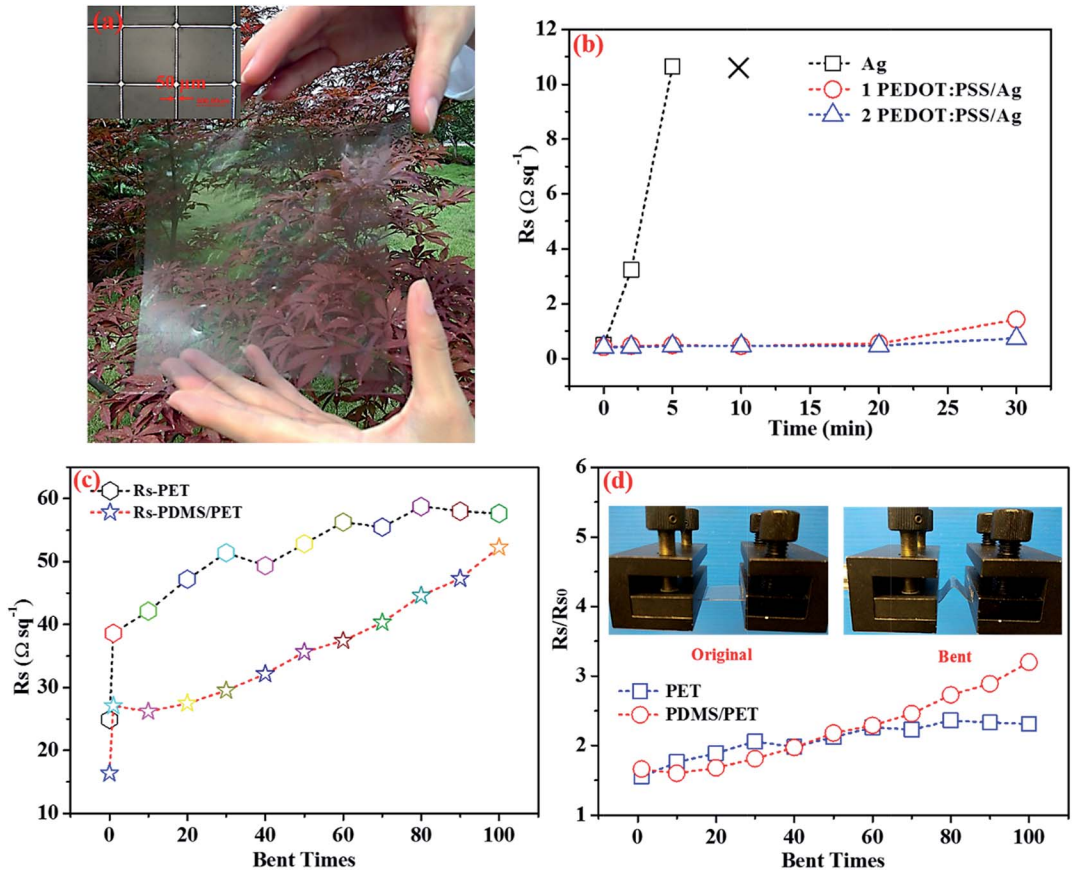


Fig. 3 (a) Photograph of a large-area Ag grid, the inset showing its optical microscopic image. (b) The sheet resistance of single Ag film, PEDOT:PSS (1 layer)/Ag film and PEDOT:PSS (2 layers)/Ag film changing with the time in UVO atmosphere. (c and d) Bending tests. Insets show photographs of PEDOT:PSS/Ag grids before and after being bent.

suitable for future flexible/wearable electronics, such as flexible, transparent and exquisite supercapacitors that can be mounted on translucent rooftops to supply energy.

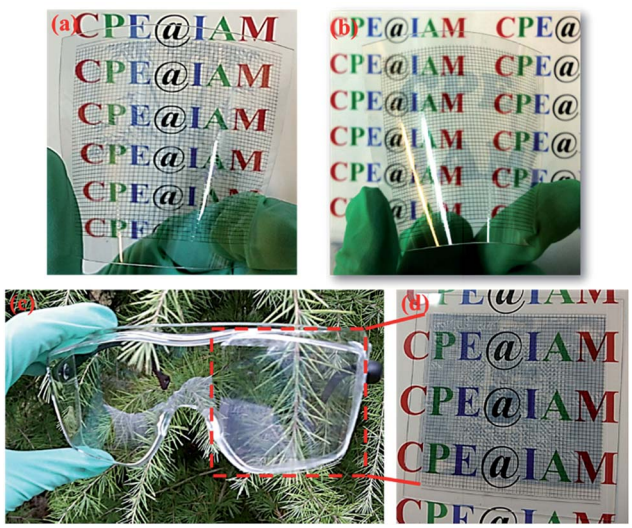


Fig. 4 Photographs of the aesthetic transparent PEDOT:PSS/Ag grids with various exquisite patterns: (a) bamboo; (b) "CPE@IAM" lab logo; (c) transparent flexible circuits on eyeglasses; (d) enlarged patterns of the circuits in (c).

Apart from superior optoelectronic performance, the electrochemical energy storage behaviour of the PEDOT:PSS/Ag grids was also investigated in flexible transparent all-solid-state supercapacitors for the first time. The PEDOT:PSS/Ag grids not only served as the current collectors but also as the active electrode material without any other capacitive materials, such as carbon materials, metal oxides, *etc.* The supercapacitor was designed to possess a symmetrical sandwiched structure, namely the electrolyte layer was sandwiched between two identical PEDOT:PSS/Ag grid electrode layers, as illustrated in Fig. 5a. As reported in our previous work,[37] a PEDOT:PSS solution with 6 vol% EG and 2 vol% surfactant exhibited relatively high electrochemical performance which could be further improved *via* increasing the thickness of the PEDOT:PSS layer. Fig. 6a shows the cyclic voltammetry (CV) curves of the supercapacitors based on the PEDOT:PSS electrodes with different layers at a constant scan rate of 100 mV s$^{-1}$. Apparently, the current density of the supercapacitors increased with the number of PEDOT:PSS layers. The galvanostatic charge–discharge (GCD) curves (Fig. 6b) at a constant current density of 0.025 mA cm$^{-2}$ showed the discharging time also increased with the layer number. The improved electrochemical performance with increasing PEDOT:PSS layers was mainly ascribed to two aspects: the PEDOT:PSS electrodes with more layers exhibited lower sheet resistance (Fig. S10†), which

was favourable for the transportation and the collection of the carriers; the active material, namely PEDOT, increased with the number of layers. Fig. S11† shows the CV and GCD curves of the supercapacitor based on PEDOT:PSS (4 layers) electrodes. The nearly rectangular shape at a high scan rate of 500 mV $s^{-1}$ and the typical triangular shape of the GCD curves both demonstrated that the supercapacitors possessed excellent capacitor behaviours. Various layers of PEDOT:PSS were further coated on the Ag grids to serve as the electrodes for supercapacitors. Fig. 6c and d show the CV curves (at a scan rate of 100 mV $s^{-1}$) and the GCD curves (at a current density of 0.025 mA $cm^{-2}$) of the supercapacitors based on various PEDOT:PSS/Ag grid electrodes. The current density and the discharging time were simultaneously increased compared with the supercapacitors based on PEDOT:PSS electrodes, which was mainly because the Ag grids improved the electrical conductivity of the PEDOT:PSS, favourable for the transportation and the collection of ions. Fig. 6e and f show the CV and GCD curves of the supercapacitor based on PEDOT:PSS (3 layers)/Ag grid electrodes. The areal specific capacitance ($C$), energy density ($E$) and power density ($P$) can be calculated using the following equations:

$$C_t = \frac{I\Delta t}{S\Delta V} \quad (4)$$

$$C_{sc} = 4C_t \quad (5)$$

$$E = \frac{1}{2}C_t\Delta V^2 \quad (6)$$

$$P = \frac{E}{\Delta t} \quad (7)$$

where $C_t$ is the specific capacitance of the supercapacitor; $C_{sc}$ is the specific capacitance of the electrode; $I$ is the discharge current; $\Delta t$ is the discharging time; $S$ is the effective area; and $\Delta V$ is the voltage window. As calculated from Fig. 6b, the areal specific capacitances of the supercapacitors based on one, two, three and four layers of PEDOT:PSS were 0.23 mF $cm^{-2}$, 0.41 mF $cm^{-2}$, 0.66 mF $cm^{-2}$, and 1.18 mF $cm^{-2}$ and the corresponding areal specific capacitances of the electrode were 0.92 mF $cm^{-2}$, 1.64 mF $cm^{-2}$, 2.64 mF $cm^{-2}$, and 4.72 mF $cm^{-2}$, respectively. Interestingly, the areal specific capacitances of the supercapacitors based on various PEDOT:PSS/Ag grid electrodes (Ag grids coated with two, three and four layers of PEDOT:PSS, respectively) were dramatically enhanced to 0.71 mF $cm^{-2}$, 1.13 mF $cm^{-2}$, and 1.84 mF $cm^{-2}$ and the corresponding areal specific capacitances of the electrode were increased to 2.84 mF $cm^{-2}$, 4.52 mF $cm^{-2}$, and 7.36 mF $cm^{-2}$, respectively. The energy density and the power density of the supercapacitor based on the PEDOT:PSS electrodes with four layers were 0.38 mW h $cm^{-2}$ and 0.036 W $cm^{-2}$ respectively while those of the supercapacitor based on the PEDOT:PSS (4 layers)/Ag grid electrodes were 0.59 mW h $cm^{-2}$ and 0.036 W $cm^{-2}$, respectively. Consequently, the areal specific capacitance and the energy density of the supercapacitors based on PEDOT:PSS/Ag grid electrodes were higher than those of the supercapacitors based on PEDOT:PSS electrodes. This was mainly because the addition of silver grids could significantly enhance the electrical conductivity and reduce the resistance of PEDOT:PSS, which was favourable for the effective transportation and the collection of the electrolyte.[38] Thus, the current density (CV curves) of the PEDOT:PSS/Ag grid-based supercapacitors was higher than that of PEDOT:PSS-based supercapacitors at the same scan rates (Fig. 6a and c). The discharging time (GCD curves) was also increased compared with the supercapacitors based on

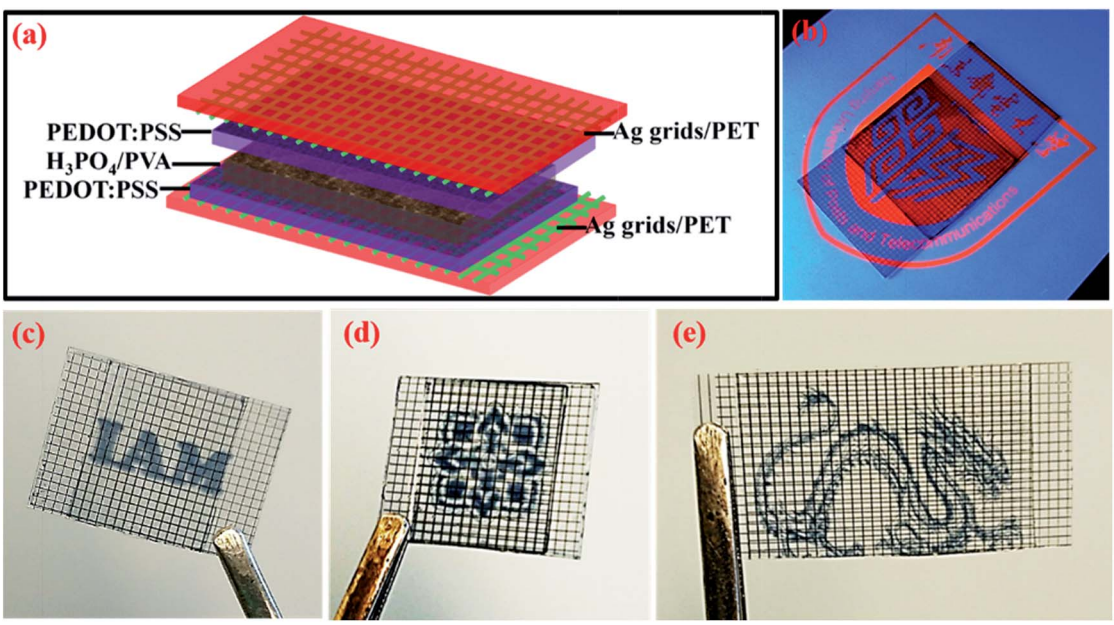


Fig. 5 (a) The structure of the supercapacitor. (b) Photograph of a translucent supercapacitor using PEDOT:PSS (3 layers)/Ag grids as electrodes. (c–e) Photographs of the aesthetic supercapacitors with various exquisite patterns.

PEDOT:PSS electrodes (Fig. 6b and d), leading to higher areal specific capacitance and larger energy density for the supercapacitors based on PEDOT:PSS/Ag grid electrodes in comparison to those of the supercapacitors based on PEDOT:PSS electrodes.

Although increasing the thickness of PEDOT:PSS improved the areal specific capacitance and the energy density, it reduced the optical transparency of the supercapacitors. Ag grids combined with 2–4 layers of PEDOT:PSS are probably the most ideal electrodes for supercapacitors that simultaneously show comparatively superior electrochemical performance and high optical transparency. For example, the comparatively high $C_t$ and $C_{sc}$ of the supercapacitor based on PEDOT:PSS (3 layers)/Ag grid electrodes were 1.13 mF cm$^{-2}$ and 4.52 mF cm$^{-2}$ respectively, which were comparable to some best performing supercapacitors previously reported.[8,39–43] Besides the superior electrochemical performance, the supercapacitor based on PEDOT:PSS (3 layers)/Ag grid electrodes also exhibited comparatively high optical transparency, as illustrated in Fig. 5b. Additionally, the CV curves (at a scan rate of 100 mV s$^{-1}$) remained almost unchanged when the supercapacitor was bent to various degrees (0°, 60°, 120° and 180°), suggesting that the

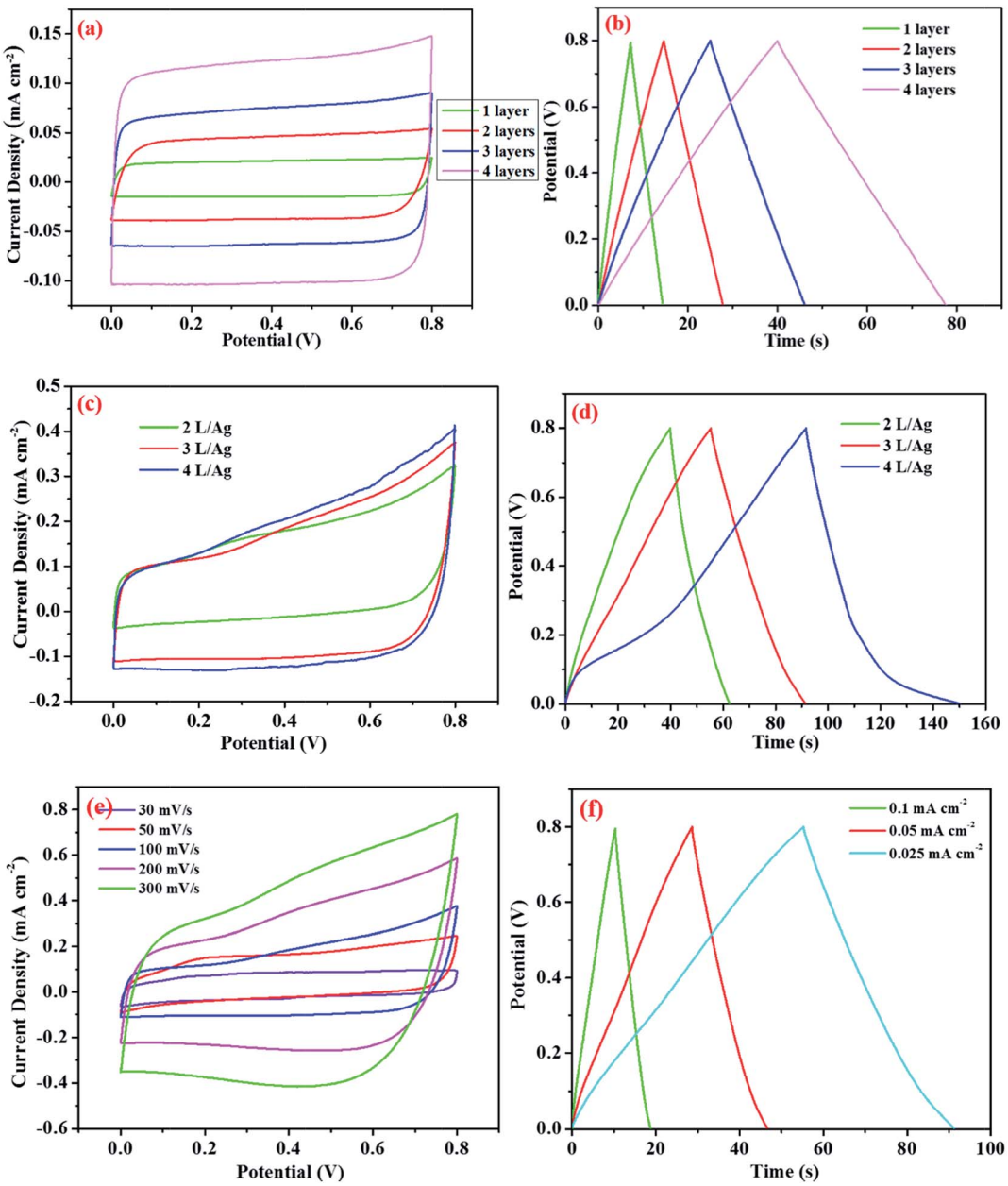


Fig. 6 Electrochemical test. (a) CV curves of supercapacitors based on PEDOT:PSS electrodes with different number of layers at constant scan rate of 100 mV s$^{-1}$. (b) GCD curves of the supercapacitors based on PEDOT:PSS electrodes with different number of layers at current density of 0.025 mA cm$^{-2}$. (c) CV curves of the supercapacitors based on various PEDOT:PSS/Ag grid electrodes at constant scan rate of 100 mV s$^{-1}$. (d) GCD curves of the supercapacitors based on various PEDOT:PSS/Ag grid electrodes at current density of 0.025 mA cm$^{-2}$. (e) CV and (f) GCD curves of the supercapacitor based on PEDOT:PSS (3 layers)/Ag grid electrodes.

supercapacitor possessed superior flexibility, as shown in Fig. S12.† As illustrated in Fig. S13,† a long-term cycle stability test was performed at a current density of 0.025 mA $cm^{-2}$ for 5000 cycles, and about 83.7% of the specific capacitance was retained, demonstrating superior cycle stability. The slight reduction of the specific capacitance during the cycling test can probably be attributed to two aspects: on the one hand, the heat generated during the cycles led to the loss of water from the PVA/$H_3PO_4$ gel electrolyte;[28] on the other hand, PEDOT partly suffered from degradation and shrinkage upon exposure to electrolyte during the repeated cycles.[44]

More intriguingly, by means of employing the inkjet-printed PEDOT:PSS/Ag grids with symmetrical patterns, aesthetic supercapacitors with various designs, such as logos, flowers and dragons, were fabricated, as shown in Fig. 5c–e. The superior flexibility, relatively high optical transparency as well as the aesthetic appearance of the supercapacitors defined their fascinating multi-functionality, enabling their application as integrated power sources for automobiles and buildings, as beautiful artworks for room decorations, and as power supplies for the flourishing flexible and wearable consumer electronic devices.

## Conclusions

Flexible transparent PEDOT:PSS/Ag grids with superior optoelectronic performance, very good electrochemical energy storage behaviours, high flexibility and aesthetic appearance have been fabricated *via* a facile, fast and low-cost inkjet-printing methodology. The ideal balance between electrical conductivity and optical transmittance was successfully achieved *via* reducing the line width, modulating the pitch of the Ag grids as well as combining with a modified PEDOT:PSS layer. The incorporation of the Ag grids with the PEDOT:PSS layer not only compensated for the demerits of single materials but also fully exploited their advantages. The Ag grids and the PEDOT:PSS layer offered extra conductive paths for each other, yielding a much lower sheet resistance of the PEDOT:PSS/Ag grids than that of either the Ag grids or the PEDOT:PSS layer, thus improving the electrochemical performance as well. The PEDOT:PSS layer could also boost the anti-oxidation capability as well as smoothen the line of the Ag grids. Various exquisite patterns of the modified PEDOT:PSS were inkjet printed on the delicate Ag grids, forming an aesthetic appearance. The superior optoelectronic performance, very good electrochemical performance, high flexibility and the aesthetic patterns of the resultant PEDOT:PSS/Ag grids greatly expand their application ranges, which are not only suitable for optoelectronic devices but also for flexible and transparent energy storage devices. As a device demonstration, flexible and transparent supercapacitors with aesthetic appearance, comparatively high optical transparency and superior electrochemical performance have been fabricated for the first time using the inkjet-printed PEDOT:PSS/Ag grids as both current collectors and electrode materials, which paves the way to fully inkjet-printed wearable and transparent energy storage devices.

## Acknowledgements

We acknowledge financial support of the National Key Basic Research Program of China (973 Program, 2014CB648300), the National Natural Science Foundation of China (21422402, 20904024, 51173081, 61136003), the Natural Science Foundation of Jiangsu Province (BK20140060, BK20130037, BM2012010), Program for Jiangsu Specially-Appointed Professors (RK030STP15001), Program for New Century Excellent Talents in University (NCET-13-0872), Specialized Research Fund for the Doctoral Program of Higher Education (20133223110008 and 20113223110005), the Synergetic Innovation Center for Organic Electronics and Information Displays, the Priority Academic Program Development of Jiangsu Higher Education Institutions (PAPD), the NUPT "1311 Project", the Six Talent Plan (2012XCL035), the 333 Project (BRA2015374) and the Qing Lan Project of Jiangsu Province.

## Notes and references

1 J. Ni, S. Fu, C. Wu, J. Maier, Y. Yu and L. Li, *Adv. Mater.*, 2016, **28**, 2259.
2 S. Fu, J. Ni, Y. Xu, Q. Zhang and L. Li, *Nano Lett.*, 2016, **16**, 4544.
3 N. Yabuuchi, K. Kubota, M. Dahbi and S. Komaba, *Chem. Rev.*, 2014, **114**, 11636.
4 J. Ni, S. Fu, C. Wu, Y. Zhao, J. Maier, Y. Yu and L. Li, *Adv. Energy Mater.*, 2016, **6**, 1502568.
5 T. Cheng, Y. Zhang, W.-Y. Lai and W. Huang, *Adv. Mater.*, 2015, **27**, 3349.
6 Y. Yu, C. Yan and Z. Zheng, *Adv. Mater.*, 2014, **26**, 5508.
7 F. Guo, P. Kubis, T. Przybilla, E. Spiecker, A. Hollmann, S. Langner, K. Forberich and C. J. Brabec, *Adv. Energy Mater.*, 2015, **5**, 1401779.
8 T. Chen, Y. Xue, A. K. Roy and L. Dai, *ACS Nano*, 2014, **8**, 1039.
9 C.-C. Chen, L. Dou, R. Zhu, C.-H. Chung, T.-B. Song, Y. B. Zheng, S. Hawks, G. Li, P. S. Weiss and Y. Yang, *ACS Nano*, 2012, **6**, 7185.
10 R. Betancur, P. Romero-Gomez, A. Martinez-Otero, X. Elias, M. Maymo and J. Martorell, *Nat. Photonics*, 2013, **7**, 995.
11 H. Y. Jung, M. B. Karimi, M. G. Hahm, P. M. Ajayan and Y. J. Jung, *Sci. Rep.*, 2012, **2**, 773.
12 Y. Z. Zhang, Y. Wang, T. Cheng, W.-Y. Lai, H. Pang and W. Huang, *Chem. Soc. Rev.*, 2015, **44**, 5181.
13 B.-U. Hwang, J.-H. Lee, T. Q. Trung, E. Roh, D.-I. Kim, S.-W. Kim and N.-E. Lee, *ACS Nano*, 2015, **9**, 8801.
14 H. Pang, Y. Zhang, W.-Y. Lai and W. Huang, *Nano Energy*, 2015, **15**, 303.
15 S. Shi, C. Xu, C. Yang, Y. Chen, J. Liu and F. Kang, *Sci. Rep.*, 2013, **3**, 2598.
16 S. Han, S. Hong, J. Ham, J. Yeo, J. Lee, B. Kang, P. Lee, J. Kwon, S. S. Lee, M. Y. Yang and S. H. Ko, *Adv. Mater.*, 2014, **26**, 5808.
17 T. Cheng, Y.-Z. Zhang, W.-Y. Lai, Y. Chen, W.-J. Zeng and W. Huang, *J. Mater. Chem. C*, 2014, **2**, 10369.

 

18 D. Angmo, T. R. Andersen, J. J. Bentzen, M. Helgesen, R. R. Sondergaard, M. Jorgensen, J. E. Carle, E. Bundgaard and F. C. Krebs, *Adv. Funct. Mater.*, 2015, **25**, 4539.
19 J. Song, J. Li, J. Xu and H. Zeng, *Nano Lett.*, 2014, **14**, 6298.
20 J. Liang, L. Li, X. Niu, Z. Yu and Q. Pei, *Nat. Photonics*, 2013, **7**, 817.
21 G. Yu, X. Xie, L. Pan, Z. Bao and Y. Cui, *Nano Energy*, 2013, **2**, 213.
22 S. Bae, H. Kim, Y. Lee, X. Xu, J. S. Park, Y. Zheng, J. Balakrishnan, T. Lei, H. R. Kim, Y. I. Song, Y. J. Kim, K. S. Kim, B. Ozyilmaz, J. H. Ahn, B. H. Hong and S. Iijima, *Nat. Nanotechnol.*, 2010, **5**, 574.
23 N. Kim, S. Kee, S. H. Lee, B. H. Lee, Y. H. Kahng, Y. R. Jo, B. J. Kim and K. Lee, *Adv. Mater.*, 2014, **26**, 2268.
24 J. P. Thomas and K. T. Leung, *Adv. Funct. Mater.*, 2014, **24**, 4978.
25 Y. H. Kim, C. Sachse, M. L. Machala, C. May, L. Müller-Meskamp and K. Leo, *Adv. Funct. Mater.*, 2011, **21**, 1076.
26 S. Hong, J. Yeo, G. Kim, D. Kim, H. Lee, J. Kwon, H. Lee, P. Lee and S. H. Ko, *ACS Nano*, 2013, **7**, 5024.
27 H. Wu, D. Kong, Z. Ruan, P.-C. Hsu, S. Wang, Z. Yu, T. J. Carney, L. Hu, S. Fan and Y. Cui, *Nat. Nanotechnol.*, 2013, **8**, 421.
28 Z. Li, G. Ma, R. Ge, F. Qin, X. Dong, W. Meng, T. Liu, J. Tong, F. Jiang, Y. Zhou, K. Li, X. Min, K. Huo and Y. Zhou, *Angew. Chem., Int. Ed.*, 2016, **55**, 979.
29 J. Liang, L. Li, K. Tong, Z. Ren, W. Hu, X. Niu, Y. Chen and Q. Pei, *ACS Nano*, 2014, **8**, 1590.
30 P. Lee, J. Ham, J. Lee, S. Hong, S. Han, Y. D. Suh, S. E. Lee, J. Yeo, S. S. Lee, D. Lee and S. H. Ko, *Adv. Funct. Mater.*, 2014, **24**, 5671.
31 G. Cai, P. Darmawan, M. Cui, J. Wang, J. Chen, S. Magdassi and P. S. Lee, *Adv. Energy Mater.*, 2016, **6**, 1501882.
32 J. Lee, P. Lee, H. B. Lee, S. Hong, I. Lee, J. Yeo, S. S. Lee, T.-S. Kim, D. Lee and S. H. Ko, *Adv. Funct. Mater.*, 2013, **23**, 4171.
33 T. Gao, Z. Li, P.-S. Huang, G. J. Shenoy, D. Parobek, S. Tan, J.-K. Lee, H. Liu and P. W. Lee, *ACS Nano*, 2015, **9**, 5440.
34 W. K. Kim, S. Lee, D. Hee Lee, I. Hee Park, J. Seong Bae, T. Woo Lee, J. Y. Kim, J. Hun Park, Y. Chan Cho, C. Ryong Cho and S. Y. Jeong, *Sci. Rep.*, 2015, **5**, 10715.
35 L. Mao, Q. Chen, Y. Li, Y. Li, J. Cai, W. Su, S. Bai, Y. Jin, C.-Q. Ma, Z. Cui and L. Chen, *Nano Energy*, 2014, **10**, 259.
36 J. Schneider, P. Rohner, D. Thureja, M. Schmid, P. Galliker and D. Poulikakos, *Adv. Funct. Mater.*, 2016, **26**, 833.
37 T. Cheng, Y.-Z. Zhang, J.-D. Zhang, W.-Y. Lai and W. Huang, *J. Mater. Chem. A*, 2016, **4**, 10493.
38 W. Liu, C. Lu, X. Wang, R. Y. Tay and B. K. Tay, *ACS Nano*, 2015, **9**, 1528.
39 T. M. Higgins and J. N. Coleman, *ACS Appl. Mater. Interfaces*, 2015, **7**, 16495.
40 Y. Meng, Y. Zhao, C. Hu, H. Cheng, Y. Hu, Z. Zhang, G. Shi and L. Qu, *Adv. Mater.*, 2013, **25**, 2326.
41 J. Ren, L. Li, C. Chen, X. Chen, Z. Cai, L. Qiu, Y. Wang, X. Zhu and H. Peng, *Adv. Mater.*, 2013, **25**, 1155.
42 X. Chen, H. Sun, Z. Yang, G. Guan, Z. Zhang, L. Qiu and H. Peng, *J. Mater. Chem. A*, 2014, **2**, 1897.
43 Z.-S. W. Z. Liu, K. Parvez, X. Feng and K. Müllen, *Adv. Mater.*, 2015, **27**, 3669.
44 S. Cho, M. Kim and J. Jang, *ACS Appl. Mater. Interfaces*, 2015, **7**, 10213.